Statistical physical theory of mode-locking laser generation with a frequency comb

F. Antenucci,[1,2] M. Ibáñez Berganza,[3] and L. Leuzzi[1,2]

[1]*NANOTEC-CNR, Institute of Nanotechnology, Soft and Living Matter Laboratory, Rome, Piazzale Aldo Moro 5, I-00185 Rome, Italy*

[2]*Dipartimento di Fisica, Università di Roma "Sapienza," Piazzale Aldo Moro 5, I-00185 Rome, Italy*

[3]*INFN, Gruppo Collegato di Parma, via G. P. Usberti, 7/A, I-43124 Parma, Italy*

(Received 29 September 2014; published 7 April 2015)

A study of the mode-locking lasing pulse formation in closed cavities is presented within a statistical-mechanical framework where the onset of laser coincides with a thermodynamic phase transition driven by the optical power pumped into the system. Electromagnetic modes are represented by classical degrees of freedom of a Hamiltonian model at equilibrium in an effective ensemble corresponding to the stationary laser regime. By means of optimized Monte Carlo numerical simulations, the system properties are analyzed while varying mode interaction dilution, gain profile, and number of modes. Properties of the resulting mode-locking laser phase are presented that were not observed in previous approaches based on mean-field approximations. For strong dilution of the nonlinear interaction network, power condensation occurs as the total optical intensity is taken by a few electromagnetic modes, whose number does not depend on the size of the system. For all reported cases, laser thresholds, intensity spectra, phase waves, and ultrafast electromagnetic pulses are computed.

DOI: 10.1103/PhysRevA.91.043811 PACS number(s): 42.60.Fc, 05.10.Ln, 05.90.+m, 42.55.Ah

I. INTRODUCTION

In multimode lasers with many cavity modes, nonlinear interactions originate among modes. One notable mechanism inducing interaction is saturable absorption, i.e., the progressive depletion of low-power tails of the light pulse traveling through the cavity during each round-trip. This causes the consequent amplification of very short pulses composed of modes with *locked phases*, a phenomenon called *mode locking* [1,2]. Mode locking (ML) derives from the nonlinear synchronization constraint on the oscillations of interacting modes. Given any quadruplet of modes $\{k_1,k_2,k_3,k_4\}$, this is expressed by the frequency-matching condition (FMC):

$$|\nu_{k_1} - \nu_{k_2} + \nu_{k_3} - \nu_{k_4}| \leqslant \gamma, \tag{1}$$

where γ is the single-mode linewidth. Phase locking occurs at the ML lasing threshold and corresponds to some long-range order in the set of modes in the cavity.

We adopt a statistical-mechanical approach to describe the optical properties of stimulated light emission from cavities with a large number of modes. In this approach the generation of a multimode ML lasing regime from a fluorescent continuous-wave (cw) regime as the optical power in the cavity is increased can be characterized as a thermodynamic phase transition between a disordered phase and a phase with long-range order. The stationary laser system can be treated as a thermodynamic system at equilibrium in a thermal bath whose effective temperature is proportional to the inverse squared power pumped into the cavity [3,4]. Since the first attempt by Gordon and Fischer in the early 2000s [5], this approach has been performed in a mean-field fully connected approximation corresponding in the optical language to the so-called *narrowband approximation* (see also Refs. [3,6–8]). This consists of choosing mode frequencies in a narrow bandwidth $\Delta\nu$ around the central frequency of the cavity. The bandwidth is so narrow that the frequency interspacing $\delta\nu$ between resonant modes is less than the linewidth γ of each mode. In this way Eq. (1) is practically always satisfied and therefore is actually irrelevant in determining lasing properties.

In the present work we introduce frequency-dependent populations of modes, considering gain profiles $g(\nu)$ and the effect of nontrivial frequency matching on the mode couplings. This analysis requires us to go beyond the limits of validity of mean-field theory, and it is carried out by means of optimized Monte Carlo (MC) simulations running on Graphic Processing Units. An exhaustive numerical analysis accounting for the fluctuations induced by these new ingredients reveals that, depending on the optical system properties, on the cavity topology, and on the relative gain-to-nonlinearity strength, different thermodynamic-like phases occur. Such regimes range from a ferromagnetic-like one, where all mode phases are aligned, to a *phase-wave* one, where phases of modes at nearby frequencies are strongly correlated, although not equal to each other. The ferromagnetic behavior occurs in the low-finesse limit of the narrowband approximation. Nontrivial phase locking occurs, instead, at high finesse. In the latter case we show how, distributing the frequencies according to an optical frequency comb [9–11], intensity spectra and pulse phase delay observed in ultrashort pulses are reproduced [12].

As it will be discussed in the following, previous studies based on mean-field theory are exact only in the narrow-bandwidth case. In this paper we go beyond the mean-field approximation, accounting also for situations in which different modes exhibit different frequencies.

Our study introduces two essential ingredients. The first one is the FMC, yielding mode interaction networks that are no longer described by mean-field theory, in which nontrivial multimode emission spectra and mode phase correlations above threshold occur. The second ingredient is a *random* dilution of the interacting network, modeling possible topological disorder in arbitrary cavity structures, e.g., multicavity channels not exactly equal to each other. We will show that, as long as it is not too strong, the latter kind of dilution does not alter at all the laser transition properties. Below a certain dilution point, however, in the lasing phase the total optical power condenses into a small set of connected modes, scaling independently of the number of modes.

II. THE MODEL

Expanding the electromagnetic field in the complete base of N normal modes $\{\boldsymbol{E}_n(\boldsymbol{r}),\nu_n\}$ [13],

$$\boldsymbol{E}(\boldsymbol{r},t)=\sum_{n=1}^{N}a_n(t)e^{-2\pi\imath\nu_n t}\boldsymbol{E}_n(\boldsymbol{r})+\text{c.c.}, \tag{2}$$

the equilibrium dynamics of the time-dependent complex amplitudes $a_n(t)$ is given by the Hamiltonian [5]

$$\mathcal{H}=-\sum_{k=1}^{N}g_k|a_k|^2-J\sum_{\{k_1,k_2,k_3,k_4\}}^{\text{ML}}a_{k_1}a_{k_2}^*a_{k_3}a_{k_4}^*, \tag{3}$$

where g_k and J are chosen as real numbers, neglecting dispersion and the Kerr-lens effect. The physical meaning of the coefficients comes from the equivalence of the Hamiltonian dynamical equation with the Haus master equation [1]: $g_k=g(\nu_k)$ is the net gain profile, and J is the self-amplitude modulation (SAM) coefficient. The ML sum runs over a subset of quadruplets such that for each element (k_1,k_2,k_3,k_4) the FMC holds. The latter implies that in the nonlinear term of Eq. (3) three nonequivalent orderings of quadruplets contribute to the sum, each one consisting of eight equivalent index permutations [14]. The Hamiltonian is symmetrized with respect to these orderings. The coupling strength in Eq. (3) is taken as $J=N/N_q$, where N_q is the number of quadruplets, making the Hamiltonian extensive.

The total optical energy stored in the system is $\mathcal{E}=N\epsilon=\sum_{k=1}^{N}|a_k|^2$, and it is kept constant in the dynamics by external power pumping. Equation (3) is a direct generalization of the Hamiltonian studied in Ref. [5] and can be seen as the ordered limit of the random laser theory analyzed in Refs. [3,7,8]. From the point of view of statistical mechanics the driven optical system composed by the cavity, the amplifying medium, *and* the optical power pumped into the system can be described by Eq. (3), which can be considered the Hamiltonian of a system at equilibrium with an effective thermal bath. The role of the inverse temperature is played by the pumping rate squared: $\mathcal{P}^2=\beta J\epsilon^2$. Here $\beta=1/k_bT$ is the inverse *heat-bath* temperature, which regulates spontaneous emission. It is usually represented as white noise in Langevin dynamics [3–8,15,16].

III. MODE INTERACTION NETWORK

Thermodynamic phases are determined by the interaction network as well. In the following we will analyze networks with varying degrees of dilution. This will be expressed as the number of quadruplets N_q vs the number of modes N. We will discuss data for $N_q=O(N^t)$, $t=1,2,3,4$.

Two essentially different types of topologies will be investigated, depending on whether the frequency bandwidth is narrow or finite. Both topologies can be further diluted upon homogeneously randomly removing quadruplets. The narrow-bandwidth topology (NBT) is *low finesse*, i.e., $\delta\nu\ll\gamma$, and the role of frequencies is irrelevant. The fully connected instance, consisting of $N_q=N(N-1)(N-2)(N-3)/8$ interacting quadruplets, corresponds to a closed Fabry-Pérot-like cavity where all longitudinal modes are localized in the same spatial region. Possible random diluted NBTs correspond to more complicated geometries, including multichannels setups. For finite bandwidth, instead, we will work in the *high-finesse* limit, $\delta\nu\gg\gamma$, with sets of equispaced frequencies [9–11,17,18]. We will term this a frequency comb topology (FCT). In this case the list of quadruplets is extracted from those nontrivially satisfying Eq. (1): modes are not all equivalent to each other, and mean-field theory does not hold.

IV. NUMERICAL SIMULATIONS AND DATA ANALYSIS

We performed extensive Monte Carlo simulations of equilibrium dynamics by means of the exchange MC [19] algorithm and the synchronous, fully parallel MC [20–23]. The latter, indeed, remarkably turns out to reproduce reliable dynamics in the present model [24]. In the NBT, system sizes from $N=25$ to 500 have been simulated for random dilutions of $N_q=O(N^t)$, $t=2,3,4$ [25]. For the FCT, we simulated systems of size $N=100-1000$ with the number of frequencies $N_f=N$ in each case and $N_q=O(N^2)$ and $O(N^3)$ upon applying the FMC filter.

The gain $g(\nu_n)$ is taken as Gaussian with varying mean-square displacement. We checked thermal equilibration, i.e., the onset of the pumped stationary regime, by looking at the energy relaxation and at the symmetry of the distribution of complex amplitude values deep in the lasing phase. In the following we present our results about (i) laser threshold identification, (ii) intensity spectra, and (iii) phase waves, electromagnetic pulses, and their correlations.

A. Laser threshold

The estimate of the laser threshold is obtained from the finite-size scaling (FSS) analysis of the behavior of the energy vs pumping rate, as shown in Fig. 1 for the FCT (for the NBT, the energy behavior is the same). For low $\mathcal{P}$ the system is in an incoherent continuous-wave regime with uncorrelated phases and zero energy per mode. As $\mathcal{P}$ increases, a phase transition occurs, as indicated by a discontinuity in the energy. For the NBT the $N\to\infty$ critical point is analytically known

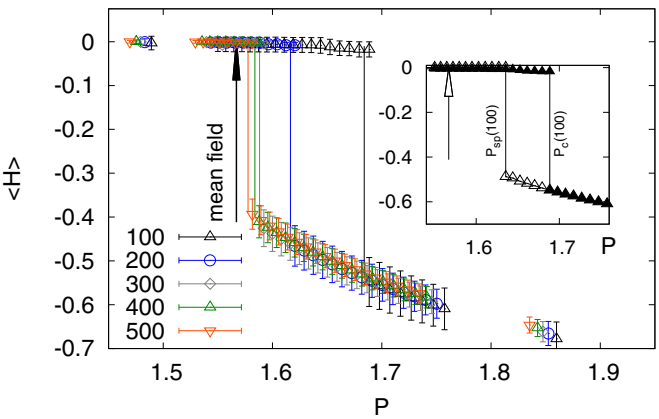

FIG. 1. (Color online) Energy vs $\mathcal{P}$ (in arbitrary units) in the frequency-comb case with $N_q\propto N^2$. The arrow marks the analytic critical point in the thermodynamic limit of the NBT. In the inset, for $N=N_f=100$ modes the spinodal line $\mathcal{P}_{\text{sp}}$ is shown next to the threshold critical line.

TABLE I. Critical point for $N \to \infty$ in various dilutions.

ν band	Narrow band				Frequency comb	
N_q	N^2	N^3	N^4	Exact	N^2	N^3
$\mathcal{P}_c$	1.56(3)	1.59(9)	1.6(3)	1.566 97	1.558(8)	1.57(1)

[3] and pointed out by an arrow in Fig. 1. For $N_q = O(N^t)$, $t = 2,3,4$, the FSS of the discontinuity point is compatible with the fully connected analytical limit, as reported in Table I. The critical thresholds for the FCT case, estimated using FSS for $N_q = O(N^2)$ and for $N_q = O(N^3)$, are reported in Table I. The cw-ML laser phase transition is first order: in the inset of Fig. 1 both the spinodal and the critical points are displayed, e.g., for $N = 100$ in a FCT. Spinodal points occur both in NBT and in FCT. In Fig. 2 the average mode magnitudes $r \equiv \langle|a|\rangle/\sqrt{\epsilon}$ are plotted. This is $\sqrt{2/\pi}$ for randomly independently oscillating amplitudes, and it discontinuously increases at the ML lasing threshold, indicating intensity mode locking. For $\mathcal{P} \to \infty$, r tends to 1 in the NBT and to 0.990(1) in the FCT case.

Power condensation

As the dilution is strong, i.e., $N_q = O(N)$, each mode interacts in an $O(1)$ number of quadruplets. Above the threshold the total power $\mathcal{E}$ turns out to be taken by a small number of connected modes, and the probability to find a configuration with energy equipartition is negligible in the thermodynamic limit. In the mean-field approximation one can prove that in order to display power condensation it must be $N_q < O(N^2)$ [24], as confirmed by numerical simulations. In the following we focus on more connected networks.

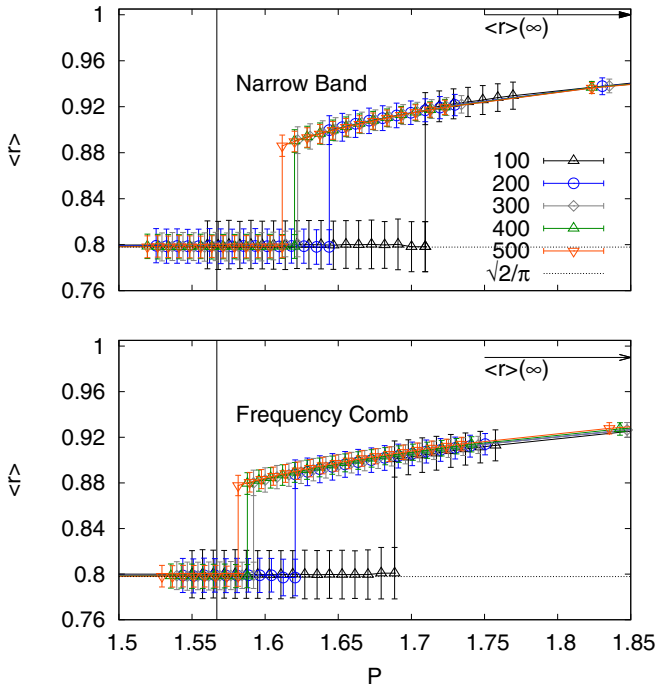

FIG. 2. (Color online) Average mode magnitude $r = \langle|a|\rangle/\sqrt{\epsilon}$ vs optical power $\mathcal{P}$ (in a.u.) for different sizes (top) in the NBT and (bottom) in the FCT.

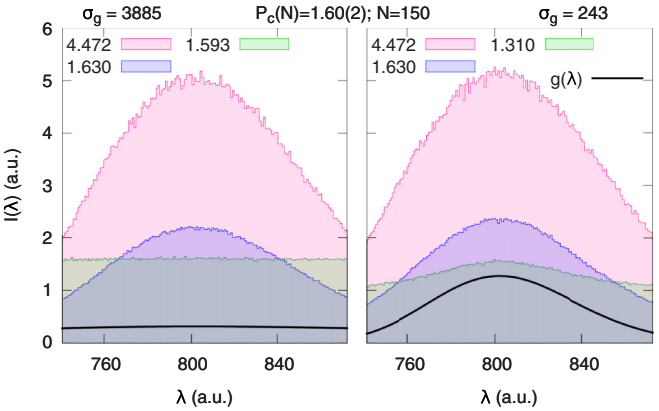

FIG. 3. (Color online) Intensity spectra for a FCT system of $N_f = N = 150$. $N_q = O(N^2)$ for increasing $\mathcal{P}$ from bottom to top. (left) Gain $g(\lambda)$ with larger variance, $\sigma_\lambda = 3885$. At $\mathcal{P} > \mathcal{P}_c$ the spectrum starts narrowing because of the nonlinear mode coupling. (right) $g(\lambda)$ with smaller variance, $\sigma_\lambda = 243$. Spectra follow the peaked gain profile already in the cw regime. At $\mathcal{P}_c$ mode locking sets in, enhancing the sharpening.

B. Intensity spectra

In Fig. 3 we show two instances of the spectra $I(\lambda_j) = \langle|a_j|^2\rangle$ vs $\lambda_j = c/\nu_j$ in FCT systems with Gaussian gain profiles with different variances. In the left panel the mean-square displacement of the gain profile in the wavelength dominion is large ($\sigma_g = 3885$) in comparison to the spectral free range, whereas in the right panel it is of the same order of magnitude ($\sigma_g = 243$). In the first case, below $\mathcal{P}$ the cw spectrum is flat and suddenly sharpens at the ML threshold $\mathcal{P}_c$. To underline this, spectra are shown right below and above $\mathcal{P}_c(N = 150) = 1.597(15)$ in Fig. 3. In the small σ_g case the spectra already appear narrower in the cw regime, following $g(\lambda)$, as displayed in the right panel of Fig. 3 for the lowest simulated pumping rate. At $\mathcal{P}_c$, however, their narrowing qualitatively changes and becomes progressively independent of $g(\lambda)$ as $\mathcal{P}$ increases, eventually taking the same spectral shape as the previous case.

We show in Fig. 3 the cumulative detections of many pulses, as in data acquisition from ultrafast ML lasers. In the MC dynamics used in the simulation, however, each MC step corresponds to a pulse generation. Within our approach it is, then, possible to look at the dynamics at much shorter time intervals, where the mode amplitude and intensity profile in λ fluctuate from pulse to pulse. This is connected to changes in the spectral phase delay of the electromagnetic pulse.

C. Electromagnetic pulses and phase delay

In terms of slow complex amplitudes [see Eq (2)], $a_n(\tau) = A_n(\tau)e^{i\phi_n(\tau)}$, $A_n = |a_n|$, the electromagnetic pulse is

$$E(t|\tau) = \sum_{n=1}^{N} A_n(\tau)e^{i[2\pi\nu_n t + \phi_n(\tau)]}. \tag{4}$$

The time $\tau \gg t$ operatively labels a single MC step in our simulations, i.e., the interval between two pulses. In Fig. 4 we show $E(t|\tau)$ at four different times τ in the dynamics. In the NBT, in the ML regime all modes acquire the same

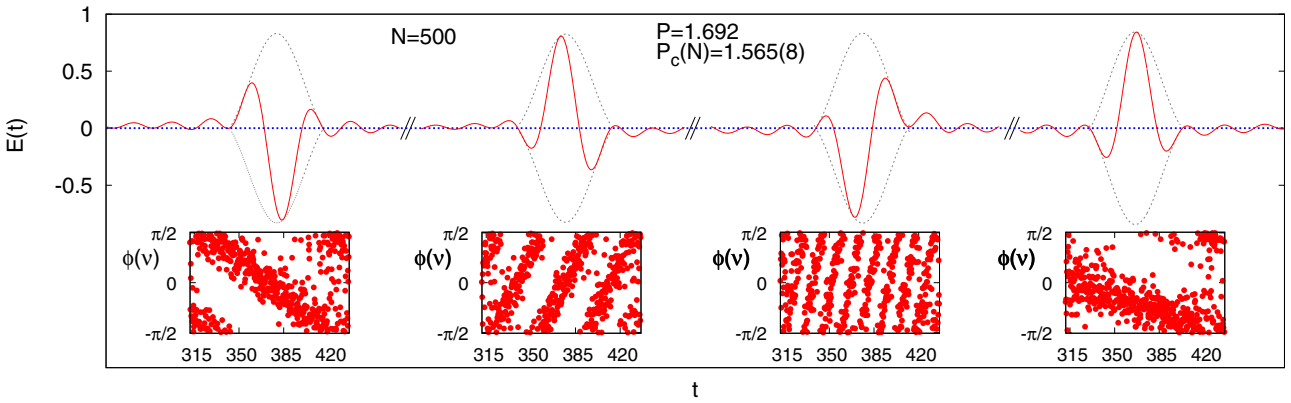

FIG. 4. (Color online) Electromagnetic field $E(t)$ at different emissions in the system dynamics with a uniform comb distribution for mode frequencies. $N = N_f = 500$. The bottom insets show phase-locked linear behavior $\phi(\nu)$ corresponding to each pulse. The phase shift in the peak of $E(t)$ with respect to the maximum of the envelope corresponds to the slope of $\phi(\nu)$. Time is in arbitrary units.

modulus and phase. In a FCT, instead, at $\mathcal{P}_c$ a nontrivial phase locking occurs, such that the mode phases exhibit a linear dependence on the mode frequencies: $\phi_n \simeq \phi_0 + \phi' \nu_n$, as shown in the bottom insets of Fig. 4. The pulse is thus unchirped [1]. The spectral *phase delay*, or group delay, $\phi' = d\phi(\nu)/d\nu|_{\nu=\nu_n}$ of the optical pulse does not depend on the frequency of mode n. It changes, however, with time τ, from pulse to pulse. Within our approach we thus find the typical spectral phase frequency profile $\phi(\nu)$ at each given pulse and its pulse-to-pulse dynamics.

1. Phase-wave lifetime

Let us define the time average over an equilibrated set of data ($\tau \geqslant \tau_{\text{therm}}$) on a time window $\mathcal{T}$: $\langle \cdots \rangle_{\mathcal{T}} \equiv \sum_{\tau=0}^{\mathcal{T}} (\cdots)/\mathcal{T}$. In the FCT, after a time $\mathcal{T} > \tau_\phi$, the average global phase correlation function $\mathcal{C}_\phi(\mathcal{T})$, defined as

$$\mathcal{C}_\phi(\mathcal{T}) \equiv \frac{1}{N_f} \sum_{\delta\nu} |C_{\delta\nu}(\mathcal{T})|\,, \tag{5}$$

$$C_{\delta\nu}(\mathcal{T}) = \frac{1}{N_f} \sum_{\nu} \langle \cos\left(\phi_\nu - \phi_{\nu+\delta\nu}\right) \rangle_{\mathcal{T}}, \tag{6}$$

is observed to decay to zero. This is at odds with the NBT, where, in the high-power regime, $C_\phi(\mathcal{T})$ is finite also for $\mathcal{T} \to \infty$. For the FCT, the distribution of correlation times τ_ϕ as the optical power varies across the lasing threshold is sharply peaked around its logarithmic average $\overline{\ln \tau_\phi}$ below threshold (see Fig. 5). For increasing $\mathcal{P} > \mathcal{P}_c$ the distribution tends to a flat curve.

2. Vanishing two-mode correlators

A related phenomenon is that the average over $\mathcal{T} > \tau_\phi$ of two-mode phase correlations $C_{\delta\nu}(\mathcal{T})$ [see Eq. (6)] vanishes, as shown in Fig. 6, implying a zero ensemble average. This occurs even though modes with frequencies ν, $\nu' = \nu + \delta\nu$ *are* correlated at each time τ (see bottom insets of Fig. 4) and $C_{\delta\nu}(\mathcal{T}) \neq 0$ when $\mathcal{T} \lesssim \tau_\phi$. In Fig. 6 we show $C_{\delta\nu}(\mathcal{T})$ as a function of $\delta\nu = \nu' - \nu$ for $\mathcal{T} = 10^4$ and $\mathcal{T} = 10^5$. In the top panel, at the shorter time window $\mathcal{T} = 10^4$, one clearly observes that $C_{\delta\nu}$ is completely uncorrelated independent of $\delta\nu$ for $\mathcal{P} < \mathcal{P}_c$. As the pumping increases above the threshold, $C_{\delta\nu}$ displays a nontrivial behavior as a function of $\delta\nu$. Above threshold, thus, the global phase correlation function $\mathcal{C}_\phi$ [see Eq. (5)] becomes larger the higher the pumping is. In other words, the correlation time τ_ϕ grows with $\mathcal{P}$ and overcomes $\mathcal{T}$: $\tau_\phi(\mathcal{P} > \mathcal{P}_c) > 10^4$. In the bottom panel of Fig. 6 we consider, instead, a time window $\mathcal{T}$ larger than the average correlation time $\tau_\phi(\mathcal{P})$ for most of the simulated pumping values $\mathcal{P}$ (see Fig. 5): it can be observed that $C_{\delta\nu}(10^5) \simeq 0$ for practically almost all $\delta\nu$, except the smallest ones for large power. The oscillations displayed by $C_{\delta\nu}(\mathcal{T})$ in Fig. 6 in the ML laser regime are due to the fact that different phase delays are involved in the thermal average. Indeed (see bottom insets of Fig. 4), the slope of $\phi(\nu)$ changes with time τ.

The origin of the vanishing of two-mode correlators is reminiscent of symmetry conservation in gauge lattice theories [26] and will be discussed elsewhere [24]. We just mention that the main difference in the lasing regime for the two topologies is that in the NBT the global U(1) symmetry is spontaneously broken, whereas in the FCT it is conserved across the threshold.

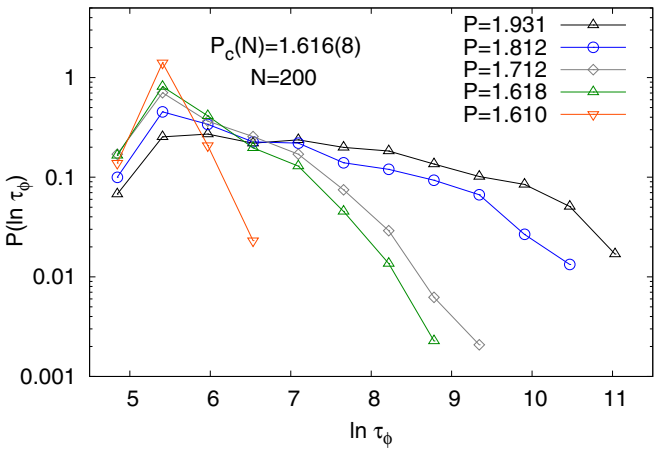

FIG. 5. (Color online) Distribution of the decay time of the equal-time phase correlation function for a system of $N = N_f = 200$ modes across the threshold $\mathcal{P}_c(N = 200) = 1.616(8)$. Time τ in is Monte Carlo steps.

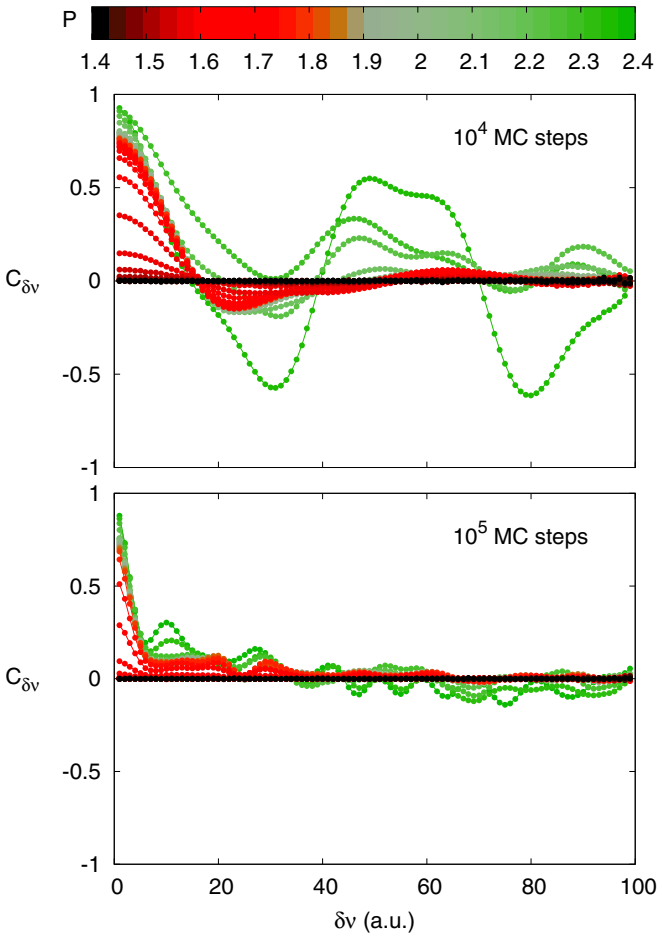

FIG. 6. (Color online) Phase-phase correlation $C_{\delta\nu}(\mathcal{T})$ as a function of frequency difference $\delta\nu = \nu' - \nu$ and optical power $\mathcal{P}$ for (top) $\mathcal{T} = 10^4$ and (bottom) $\mathcal{T} = 10^5$ in a FCT cavity with $N = 100$ and $N_q = O(N^2)$. The threshold power is $\mathcal{P}_c(100) = 1.62(2)$, and the range of power of the displayed correlations is reported on the top palette from black for low power to light green (light gray) for high power.

V. CONCLUSIONS

We presented a statistical-mechanical approach to the study of real-world ultrashort mode-locked multimode lasers in closed optical cavities, including possible degrees of topological disorder. In previous approaches, statistical-mechanical systems with distinct resonances have been studied in the mean-field approximation (see, e.g., Refs. [15,16,27]). The key point is, however, that the mean-field solution is exact only in the narrow-bandwidth limit. When describing inhomogeneous topologies, such as the frequency comb topology of equispaced well-refined resonances, the only thing that the mean-field theory can account for is a shift in the pumping threshold resulting from the dilution (in fact, just a modification of the coupling constant). The nature of the predicted mode-locked regime remains, indeed, identical to the one predicted assuming a narrow bandwidth. This limit basically lies in the very definition of the mean-field method: since the fluctuations of the mode degrees of freedom are neglected, a many-body problem is actually reduced to a one-body problem, in which all modes exhibit a common average phase and a common average intensity. The inhomogeneity in the frequency dependence of the interaction network in more realistic cases, in which modes with nearby frequencies have stronger coupling, is simply neglected by construction. Because of the mean-field assumption, previous approaches have not, and could not have, accounted for the main properties here reported: phase waves, nonequipartition threshold, and vanishing two-mode correlators.

Our approach, going beyond mean-field theory with Monte Carlo simulations of equilibrium dynamics, allows us to reproduce and study the onset of the lasing regime and the behavior of emission spectra and laser pulses and relative group phase delays at any supplied power. The existence of metastable lasing regimes marked by spinodal points in the energy behavior (see the inset of Fig. 1) accounts for the onset of optical bistability [28,29]. The phenomenon of power condensation for extreme dilution of mode interaction and the vanishing of the equal-time two-mode phase correlations for long times are properties that can be experimentally tested. Furthermore, this kind of approach opens the way to further analyze the carrier-envelop offset phase behavior and the tolerance to disorder in the coupling SAM coefficient. The latter analysis is useful, e.g., for a stabilized microresonator in chip-based devices [30,31] in which technical precision undergoes micron-size constraints and controlling material damage is a true challenge. Eventually, by including open-cavity terms [32,33] and strong disorder in the nonlinear coupling [3,6–8], our approach will be able to be applied to the study of random lasers [34–38].

ACKNOWLEDGMENTS

The authors would like to thank C. Conti, A. Crisanti, and G. Parisi for stimulating discussions. The research leading to these results has received funding from the Italian Ministry of Education, University and Research under the Basic Research Investigation Fund (FIRB/2008) program/CINECA Grant No. RBFR08M3P4 and under the PRIN2010 program, Grant No. 2010HXAW77-008, and from the People Programme (Marie Curie Actions) of the European Union's Seventh Framework Programme FP7/2007-2013 under REA Grant Agreement No. 290038, NETADIS project.

[1] H. A. Haus, IEEE J. Quantum Electron. **6**, 1173 (2000).
[2] H. A. Haus, *Waves and Fields in Optoelectronics* (Prentice-Hall, Englewood Cliffs, NJ, 1984).
[3] F. Antenucci, C. Conti, A. Crisanti, and L. Leuzzi, Phys. Rev. Lett. **114**, 043901 (2015).
[4] A. Marruzzo and L. Leuzzi, Phys. Rev. B **91**, 054201 (2015).
[5] A. Gordon and B. Fischer, Phys. Rev. Lett. **89**, 103901 (2002).
[6] L. Angelani, C. Conti, G. Ruocco, and F. Zamponi, Phys. Rev. Lett. **96**, 065702 (2006).

[7] L. Leuzzi, C. Conti, V. Folli, L. Angelani, and G. Ruocco, Phys. Rev. Lett. **102**, 083901 (2009).
[8] C. Conti and L. Leuzzi, Phys. Rev. B **83**, 134204 (2011).
[9] T. Udem, R. Holzwarth, and T. Hansch, Nature (London) **416**, 233 (2002).
[10] A. Baltuška, T. Udem, M. Uiberacker, M. Hentschel, E. Goulielmakis, C. Gohle, R. Holzwarth, V. S. Yakovlev, A. Scrinzi, T. W. Hänsch *et al.*, Nature (London) **421**, 611 (2003).
[11] A. Schliesser, C. Gohle, T. Udem, and Th. W. Hänsch, Opt. Express **14**, 5975 (2006).
[12] T. Brabec and F. Krausz, Rev. Mod. Phys. **72**, 545 (2000).
[13] M. Sargent, III, M. O'Scully, and W. E. Lamb, *Laser Physics* (Addison-Wesley, Reading, 1978).
[14] The three orderings inequivalent with respect to the FMC are $\{k_1,k_2,k_3,k_4\}$, $\{k_1,k_3,k_2,k_4\}$, and $\{k_1,k_4,k_2,k_3\}$. Given a quadruplet $\{A,B,C,D\}$, the equivalent permutations are (i) $A \leftrightarrow C$, (ii) $B \leftrightarrow D$, and (iii) $A \leftrightarrow B, C \leftrightarrow D$ and their combinations.
[15] A. Gordon and B. Fischer, Opt. Commun. **223**, 151 (2003).
[16] O. Gat, A. Gordon, and B. Fischer, Phys. Rev. E **70**, 046108 (2004).
[17] M. Bellini and T. W. Hansch, Opt. Lett. **25**, 1049 (2000).
[18] S. A. Diddams, D. J. Jones, J. Ye, S. T. Cundiff, J. L. Hall, J. K. Ranka, R. S. Windeler, R. Holzwarth, T. Udem, and T. W. Hansch, Phys. Rev. Lett. **84**, 5102 (2000).
[19] K. Hukushima and K. Nemoto, J. Phys. Soc. Jpn. **65**, 1604 (1996).
[20] P. Peretto, Biol. Cybern. **50**, 51 (1984).
[21] H. Mahmoudi and D. Saad, J. Stat. Mech. (2014) P07001.
[22] F. L. Metz and W. K. Theumann, J. Phys. A **41**, 265001 (2008).
[23] F. L. Metz and W. K. Theumann, J. Phys. A **42**, 385001 (2009).
[24] F. Antenucci, M. Ibañez Berganza, and L. Leuzzi, arXiv:1412.8610.
[25] We also tested the network-to-network fluctuations over different numbers of network realizations and found that the fluctuations $[\overline{O^2} - \overline{O}^2]^{1/2}$ of any observables O over the distribution of topologies are already one order of magnitude lower than thermal fluctuations, $[\langle O^2\rangle - \langle O\rangle^2]^{1/2}$, in the worst case of the small size $N = 100$.
[26] J. B. Kogut, Rev. Mod. Phys. **51**, 659 (1979).
[27] A. Rosen, R. Weill, B. Levit, V. Smulakovsky, A. Bekker, and B. Fischer, Phys. Rev. Lett. **105**, 013905 (2010).
[28] H. Gibbs, *Optical Bistability: Controlling Light with Light* (Elsevier, Amsterdam, 1985).
[29] A. Baas, J. P. Karr, H. Eleuch, and E. Giacobino, Phys. Rev. A **69**, 023809 (2004).
[30] C.-C. Lee, I. Hartl, C. Mohr, J. Bethge, S. Suzuki, M. E. Fermann, and T. R. Schibli, Opt. Lett. **37**, 3084 (2012).
[31] K. Saha, Y. Okawachi, S. Bonggu, J. S. Levy, R. Salem, A. R. Johnson, M. A. Foster, M. Lamont, M. Lipson, and A. L. Gaeta, Opt. Express **21**, 1335 (2013).
[32] C. Viviescas and G. Hackenbroich, Phys. Rev. A **67**, 013805 (2003).
[33] G. Hackenbroich, C. Viviescas, and F. Haake, Phys. Rev. A **68**, 063805 (2003).
[34] N. M. Lawandy, R. M. Balachandran, A. S. L. Gomes, and E. Sauvain, Nature (London) **368**, 436 (1994).
[35] H. Cao, Y. G. Zhao, H. C. Ong, S. T. Ho, J. Y. Dai, J. Y. Wu, and R. P. H. Chang, Appl. Phys. Lett. **73**, 3656 (1998).
[36] H. Cao, J. Phys. A **38**, 10497 (2005).
[37] D. S. Wiersma, Nat. Phys. **4**, 359 (2008).
[38] N. Ghofraniha, I. Viola, F. Di Maria, G. Barbarella, G. Gigli, L. Leuzzi, and C. Conti, Nat. Commun. **6**, 6058 (2015).